Assessing Local Emission for Air Pollution via Data Experiments

Yuru Zhu[1], Yinshuang Liang[3]and Song Xi Chen[1,2]

[1]Center for Statistical Science,
[2]Guanghua School of Management, Peking University, Beijing, 100871, China
[3]School of Information Engineering, Zhengzhou University of Technology, Henan, 450044, China

Key Points:

- Calm periods after sustained cleaning processes but before the arrival of transported pollutants are selected to gauge local emissions.
- Three North China cities saw significant reductions in the average hourly growth rates of $PM_{2.5}$ and SO_2, but not NO_2 in 2017 and 2018.
- Beijing's winter growth rates of $PM_{2.5}$ were comparable to those in the heavy industrialized Tangshan and Baoding, and even higher in 2018.

Corresponding author: Song Xi Chen, `csx@gsm.pku.edu.cn`

Abstract

Although air pollution is largely due to anthropogenic emission, the observed pollution levels in a city are confounded by meteorological conditions and regional transportation of pollutants. However, effective air quality management requires measures for local emissions of the city. With a data selection algorithm, we choose calm episodes after strong cleaning processes to measure the growth of three air pollutants ($PM_{2.5}$, NO_2 and SO_2) before the arrival of transported pollution. Panel data regression models are used to analyze the episode data from the quasi-experiments to quantify the local emission in three North China cities from March 2013 to February 2019. The study reveals a significant reduction in the average hourly growth rates for $PM_{2.5}$ and SO_2 in 2017-2018 as compared to the levels in 2013 in almost all seasons and cities. However, the local emission with respect to NO_2 was little changed for almost all seasons and cities. The study also finds the winter growth rates of $PM_{2.5}$ in Beijing were comparable to those in the heavy industrialized Tangshan and Baoding, even the $PM_{2.5}$ hourly growth rates for winter 2018 in Beijing were higher than those in Tangshan and Baoding, revealing Beijing's substantial emission.

1 Introduction

Air pollution is both environmental and public health issues in many countries, which is largely driven by excessive emissions due to anthropogenic activities. The purpose of air quality management is to reduce the amount of emissions. However, quantifying the amount of emission in a city or a small area is a challenging task. Emission inventory (EI) is a tool for emission measurement by enumerating human and industrial activities, which involves down-scaling larger area production and energy statistics to smaller geographical areas (Y. Huang et al., 2015; Kuykendal, 2017; Zhong et al., 2017). The inventory is usually compiled every 2-3 years which implies temporal delays in compiling the measurements, and is also subject to reporting errors.

Studies have shown air quality is much influenced by meteorology and regional transportation. Regional transport of pollutants was found to contribute to concentrations of $PM_{2.5}$ (L. T. Wang et al., 2014; Z. Wang et al., 2014; Zheng et al., 2015) and SO_2 (Yang et al., 2013) in Beijing. K. Huang et al. (2014) and L. Wang et al. (2014) showed that anomalous wind and humidity conditions were related to high $PM_{2.5}$ concentrations in Beijing. Seo et al. (2017) investigated a severe haze episode in 2014 at both an urban site in Seoul and an upwind background site on Deokjeok Island, and found warm, humid and stagnant meteorological conditions were conducive to the accumulation of pollutants and the oxidation of precursors. Su et al. (2017) found a dilution effect on the pollution by the planetary boundary layer height (BLH) which defines the aerosol vertical conditions. Su et al. (2018) conducted an analysis of the BLH and $PM_{2.5}$ concentrations over four major regions of China, and concluded that BLH was largely negatively correlated with the particulate matter concentration. An adjustment approach to removing meteorological confounding in the observed concentrations was proposed in (X. Liang et al., 2015; Zhang et al., 2020) via the nonparametric regression model and constructing a baseline meteorological distribution.

Numerical models have been constructed to account for pollutant emission, the meteorological and chemical processes, as well as their interactions on regional air quality, such as the Community Multi-Scale Air Quality (CMAQ), the Comprehensive Air Quality Model with extensions (CAMx), the PSU/NCAR Mesoscale Model (MM5) and the Weather Research and Forecast (WRF)-Chem model; see L. T. Wang et al. (2014); Xing et al. (2011) and Li et al. (2015); Titov et al. (2007); Wu et al. (2013) and Lee et al. (2009) and Tie et al. (2007) for applications in air quality assessment. The numerical models can evaluate the effectiveness of control measures via simulating different emission control scenarios. In the CAMx model, Particulate Source Apportionment Technology (PSAT)

which is a source tagging method can track the relative source contribution to pollutant concentrations (Li et al., 2015). Z. Chen et al. (2019) employed a combined CAMx, WRF, the source emission model (SMOKE) to evaluate four pollution episodes and found a dramatic decrease in SO_2 with nitrate ions being the dominant $PM_{2.5}$ component. The relative contribution of coal combustion to $PM_{2.5}$ concentrations in Beijing dropped from 40% in March 2013 to 11% in March 2018 as a result of China's "Coal to Gas" project and "2 + 26 Cities" regional air quality management strategy (MEP, 2017). T. Huang et al. (2017) compiled and analyzed a global NO_x emission inventory to explore spatial and temporal trends in emissions from 1960 to 2014, which suggested a dramatic increase in annual anthropogenic emissions of NO_x from 7.39 to 67.8 teragrams in developing countries and showed slow progress on NO_x emission control.

In the last two decades, live air quality monitoring data are increasingly available to provide timely measurements on a set of pollutants in many locations in the world. However, the data may not entirely reflect emission at a location because they are influenced by regional transportation and meteorological conditions as shown above. As revealed in X. Liang et al. (2015); Zhang et al. (2017), the air quality in the North China Plain (NCP) is governed by the northerly versus southerly wind regimes. The cleaning processes in the NCP are typically conducted by strong northerly winds that blow away the pollutants and refresh the near earth atmosphere, while southerly wind brings more polluted air mass from the southern part of the NCP which is installed with excessive heavy industrial capacities (Zheng et al., 2015).

Motivated by the geographical and meteorological reality in the NCP, we develop an algorithm to select temporal segments of the time series observations corresponding to calm periods after sustained northerly cleaning but before the arrival of the transported pollutants for three cities: Beijing, Tangshan and Baodin in the northern part of NCP. Indeed, every time after a strong northerly system thoroughly refreshes the air, it offers an opportunity to check on the growth of air pollution in a city over the quasi-experiment period of calm weather before transported pollutants are brought from the south. By applying seasonal regression for panel data with hourly dummy variables, the hourly growth rates of the three pollutants ($PM_{2.5}$, SO_2 and NO_2) from the start of the calm episodes are estimated. To remove meteorological confounding, the estimated growth rates are adjusted according to the meteorological baseline distributions based on data from 2013 to 2018.

The analysis reveals a sustained reduction trend in the adjusted average growth rates of $PM_{2.5}$ and SO_2 since 2013. Relative to the 2013 levels, the meteorologically adjusted average hourly growth rates in 2018 in Beijing were reduced by 2.9-3.7 $\mu g/m^3$ (52.9%-66.4%) in the non-winter seasons, 1.3-2.5 $\mu g/m^3$ (16.1%-31.9%) in winter for $PM_{2.5}$; and 0.6-3 $\mu g/m^3$ (65.1%-87.1%) for SO_2. Tangshan and Baoding also saw a significant reduction in the average hourly growth rates of $PM_{2.5}$ and SO_2. The reduction for $PM_{2.5}$ ranged 5.6-9.7 $\mu g/m^3$ (68.9%-78.3%) in Baoding; 0.5-1.7 $\mu g/m^3$ (14%-24.6%) for spring and summer, 5.4-7 $\mu g/m^3$ (52.5%-62.3%) for fall and winter in Tangshan. And those for SO_2 were 1.2-1.6 $\mu g/m^3$ (34.7%-52.1%) for summer and autumn, 5.9-20.2 $\mu g/m^3$ (80.9%-85.9%) for spring and winter in Baoding; 1.1-2.3 $\mu g/m^3$ (27.8%-63.3%) for non-winter seasons, 8 $\mu g/m^3$ (75.1%) for winter in Tangshan, respectively. However, the NO_2 growth rates had not been reduced in the two Hebei cities with some notable increases over the years, and for Beijing there were only some signs of reduction emerging in 2018. This reflects the air quality management strategy in North China which has been much focused on improving the coal related emission, and vehicle related emission control has lagged much behind that for coal.

2 Data and Variables

The air pollution data analyzed in this study are hourly concentrations from the so-called Guokong monitoring sites in three North China cities: Beijing, Baoding and Tangshan. The Guokong sites are directly administrated by China's Ministry of Ecology and Environment (MEE) to avoid potential local interference. We focus on the hourly $PM_{2.5}$, SO_2 and NO_2 concentrations during the constructed pollution growth episodes from six sites in Beijing, three sites in Baoding and Tangshan, respectively. Among the six Guokong sites in Beijing, there are two clusters of sites with each having three sites. One cluster is located in the northwest (hence Beijing NW), and another in the southeast of central Beijing (Beijing SE). Tangshan is a steel-making city 155 kilometers (KMs) to the east slightly south of Beijing, and Baoding is 140 KMs to the southwest of Beijing. Figure S1 of the supporting information (SI) provides a map on the northern portion of the NCP that encompasses the three cities, and Table S1 has details on the site clusters in three cities. To reduce measurement errors, we applied a five point moving average filter over the hourly time series data with weights 0.1, 0.2, 0.4, 0.2 and 0.1 for $t-2, t-1, t, t+1$ and $t+2$, respectively.

We matched each of the air quality monitoring clusters in the three cities with the nearest meteorological station from China Meteorological Administration (CMA). Specifically, two CMA stations are employed in Beijing, one for Baoding and Tangshan, respectively, as shown in Table S1. The meteorological variables include hourly measurements of the dew point temperature (DEWP), relative humidity (HUMI), air pressure (PRES) and temperature (TEMP), wind direction (W) and speed (WS), cumulative wind speed (CWS) and precipitation (R). The wind directions are grouped into five categories based on the study of X. Liang et al. (2015): northeast (NE) having NNE, NE and ENE (according to the azimuth degrees on the rose wind plot); northwest (NW) for W, WNW, NW, NNW and N; southeast (SE) including E, ESE, SE, SSE and S; southwest (SW) having SSW, SW and WSW; and CV for the calm and variable wind. The CWS at time t sums over wind speed from the first hour of a wind direction to time t under the same wind direction. Whenever there is a change of direction, CWS is set to zero and starts to accumulate under the new direction. Furthermore, we define the cumulative northerly (southerly) wind speed CNWS (CSWS) that merges NE and NW (SE and SW).

We obtained the hourly boundary layer height from the Global Reanalysis data ERA5 provided by the European Centre for Medium-Range Weather Forecasts (ECMWF) at a grid resolution of 0.5×0.5 (latitude by longitude). The grid location of the ERA5 data stream which was closest to the center of the air quality monitoring clusters was used for each site in this cluster. We took the logarithm of humidity (LogHUMI) and boundary layer height (LogBLH) to reduce the skewness of the measurements. Furthermore, we composed two pre-episode variables: the sum of hourly northerly wind speed (SNWS) and the maximum of the cumulative northerly wind speed (MCNWS) in the 24 hours before the calm episodes. These two variables reflected the extent of northerly cleaning.

The time range of the study is from March 2013 to February 2019 which spans over six seasonal years, where one seasonal year covers spring (March to May), summer (June to August), fall (September to November), and winter (December to February next year). The season is the study unit of analysis.

Figure S2 shows $PM_{2.5}$ versus the accumulated wind speed under five wind directions in four seasons in 2015 for the four site clusters. Patterns of the wind effects for other years are similar. The figure shows strong cleaning effects of the northerly winds while such effects can not be seen for southerly winds in three cities. Figure S3 reports pair-wise Spearman's rank correlation coefficients between the three pollutants ($PM_{2.5}$, SO_2 and NO_2) and the cumulative northerly (CNWS) and southerly (CSWS) wind speeds in 2015 for the four site clusters, which confirms Figure S2's revelation. The only exception is for NO_2 in the summer and the southerly wind's effect in Baoding in winter. The

latter is because Baoding is closer to the middle of the NCP, where the effect of the northerly cleaning is not as profound as in the other two cities located toward the northern edge of the NCP. In contrast, Beijing tends to be the first one among NCP cities to be scavenged by the northerly cleaning processes (Zheng et al., 2015), which makes the correlation more pronounced.

We write $\{WS_t\}_{t=1}^L$, $\{CNWS_t\}_{t=1}^L$ and $\{CSWS_t\}_{t=1}^L$ for time series of the instantaneous wind speed, the cumulative northerly and southerly wind speed, respectively, $\{R_t\}_{t=1}^L$ for the cumulative precipitation, and $\{PM2.5_t\}_{t=1}^L$ for concentrations of $PM_{2.5}$. Here L is the total length of observation time.

3 Calm Episodes

The selection of calm episodes for gauging local emissions consists of identifying three key time points: (i) the end time t_ω of northerly cleaning processes, (ii) the beginning time t_s and (iii) the ending time t_e of calm episodes. We first define $\mathcal{A}$ to be the set of ending times t_ω of northerly cleaning processes, which satisfy

$$CNWS_{t_\omega-1} \geq 10.8m/s \text{ and } CNWS_{t_\omega} = 0. \tag{3.1}$$

It is noted that $CNWS_{t_\omega} = 0$ implies a change of wind direction from the northerly, and 10.8 m/s (meters/second) corresponds to the lower limit of a strong breeze at grade 6 on the Beaufort scale. As it is cumulative northerly, it would not be restrictive.

We then locate the starting time t_s of a calm episode around each $t_\omega \in \mathcal{A}$, which corresponds to the lowest $PM_{2.5}$ in a neighborhood of t_ω within a calm, cleaned and dry period, as the purpose of the study is to investigate $PM_{2.5}$ growth characteristics after cleaning by the northerly but before the transported pollution under the southerly wind. Imposing the dryness condition is to avoid mixing the cleaning due to strong northerly wind and that by precipitation. As North China is generally dry in non-summer seasons, the dryness requirement is not restrictive.

Let $\mathcal{C}$ be the set of times when the system is calm, clean and dry satisfying

$$WS_t \leq 5.4m/s, \max\{PM2.5_{t-1}, PM2.5_t\} \leq 35\mu g/m^3, R_{t-1} = R_t = 0, \tag{3.2}$$

where the wind speed (WS_t) is confined to grades 0-3 (no more than 5.4m/s) on the Beaufort wind scale. It requires that $PM_{2.5}$ is not larger than $35\mu g/m^3$ for two consecutive hours, where $35\mu g/m^3$ is the daily threshold level for acceptable air quality in China. We replace $35\mu g/m^3$ with $50\mu g/m^3$ for Tangshan and Baoding due to more severe baseline pollution in the two cities because of heavier industrial installations in the two cities.

Let $\mathcal{E}_{t_\omega}$ be the set of the ending times of the previously selected calm episodes that end before t_ω. It starts as an empty set $\mathcal{E}_0 = \varnothing$ and is updated by adding the ending times of selected calm episodes. The start time t_s of a new episode is obtained by searching within an 8-hour neighborhood of t_ω within $\mathcal{C}$ after the ending time of the previous episode, namely

$$t_s = \arg\min_{t \in \mathcal{B}_{t_\omega}} PM2.5_t, \tag{3.3}$$

where $\mathcal{B}_{t_\omega} = [t_\omega - 8, t_\omega + 8] \cap (max\{t : t \in \{0\} \cup \mathcal{E}_{t_\omega}\}, L] \cap \mathcal{C}$. Due to the atmospheric variation and measurement errors, t_s and t_ω may not coincide as the cleaning processes can stop before or continue after t_ω. Table 1 reports the seasonal averages for $t_s - t_\omega$ for each site cluster, which shows that t_s tended to be earlier than t_ω with the differences to be the largest in winter.

After attaining a t_s, we monitor the calm episodes starting from t_s until

$$R_t = 0, CNWS_t \leq 3.3m/s \text{ and } CSWS_t \leq 13.8m/s \tag{3.4}$$

is not satisfied. The last hour such that Condition (3.4) is satisfied is the episode's ending time t_e. Condition (3.4) excludes continuous cleanings by the northerly or substantial transportation by the southerly wind, respectively. It is noted that 3.3 m/s and 13.8 m/s correspond to Beaufort wind force at grade 2 and grade 6, respectively. Grade 6 may look strong. However, again it is on the cumulative southerly wind over previous hours, hence it is not that restrictive.
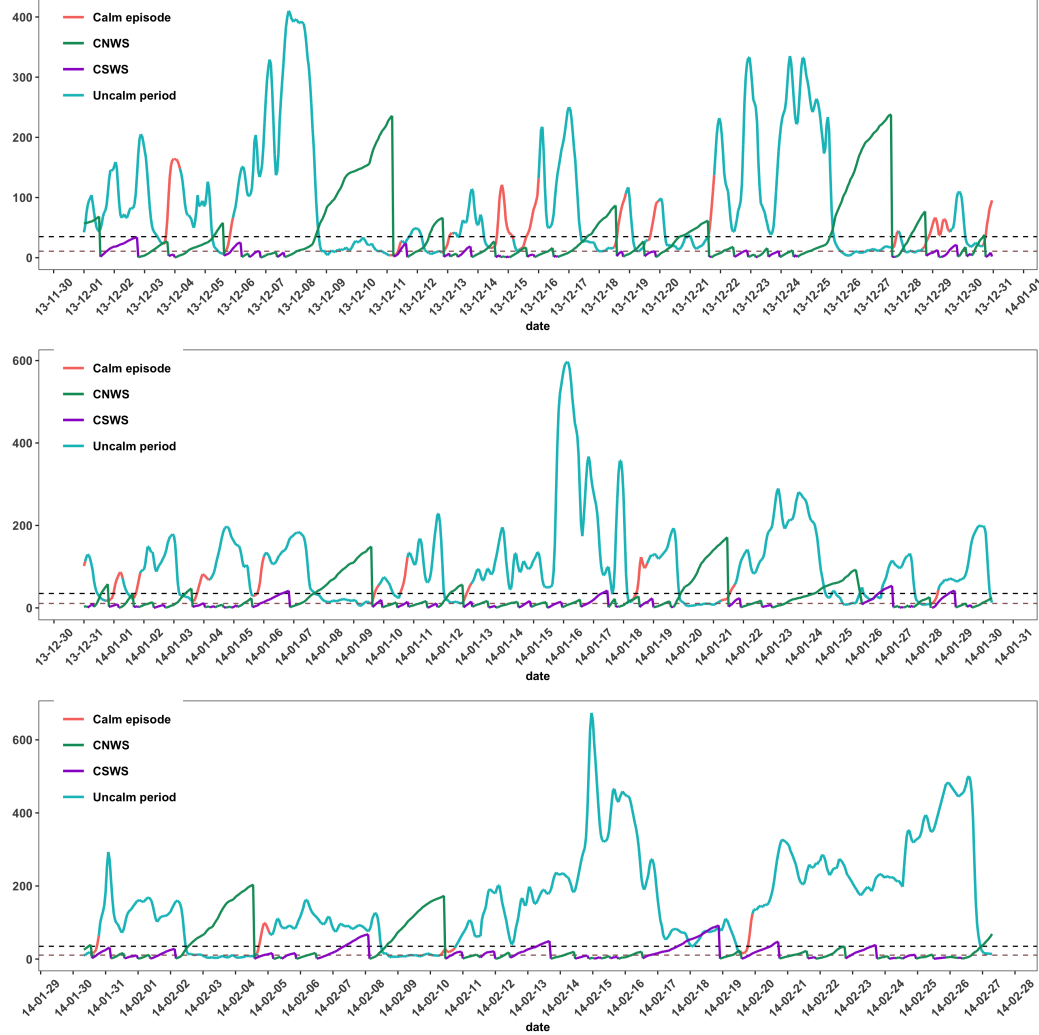

Figure 1: The time series of $PM_{2.5}$ (μg/m^3), cumulative northerly wind speed (green) and cumulative southerly (purple) wind speed (m/s) in winter of 2013 in Dongsi with observations of $PM_{2.5}$ during the calm episode shown in red, otherwise in blue. The black and brown dashed lines mark 35 μg/m^3 and 10.8 m/s, respectively.

We filtered out episodes whose length ($t_e - t_s$) is less than three hours to avoid short and unstable ones. The algorithm for calm episode selection is described in Algorithm 1 in the SI. The episodes selected in the winter of 2013 in Beijing's Dongsi site are shown in Figure 1 against the overall time series of $PM_{2.5}$ and CNWS or CSWS. The numbers of episodes and their summary statistics in the four site clusters are reported in Table 1. For clusters in Beijing and Tangshan, the number of calm episodes was largest in winter, followed by autumn, summer and spring, as northerly cleaning processes were

Cluster	Season	Count	Day	Night	Length				PM$_{2.5}$ Range	$t_s - t_\omega$	Gap Time
					Average	Q1	Q2	Q3			
Beijing SE	spring	284	187	97	7.4(0.3)	4	6	9	33(2.2)	-1.5(0.2)	122.9(7.9)
	summer	337	273	64	7.8(0.2)	5	7	10	25.7(1.3)	-0.5(0.2)	106.3(6)
	autumn	424	354	70	9.2(0.2)	6	8	12	33.6(1.3)	-1(0.1)	80.2(3.4)
	winter	494	413	81	9.3(0.2)	6	9	12	62.6(2.5)	-2.2(0.1)	67(2.4)
Beijing NW	spring	293	209	84	7.6(0.2)	4	7	10	31.8(1.8)	-1.2(0.2)	124.8(6.1)
	summer	334	273	61	9.5(0.3)	5	9	12	26.2(1.2)	-0.7(0.2)	103.2(5.7)
	autumn	409	326	83	10.7(0.3)	6	10	13	32.2(1.4)	-1.1(0.2)	82.8(3.6)
	winter	451	392	59	9.7(0.2)	7	9	12	56.1(2.4)	-2.5(0.1)	74.7(3.2)
Tangshan	spring	346	245	101	6.9(0.2)	4	6	9	37.2(1.6)	-1.5(0.2)	101.4(5.3)
	summer	313	186	127	8.5(0.3)	5	8	12	31(1.5)	-0.2(0.2)	114.3(7.5)
	autumn	443	356	87	10.5(0.3)	6	10	14	45.8(2)	-1.6(0.1)	71.1(3.6)
	winter	533	432	101	9.2(0.2)	5	8	12	56.1(2.1)	-1.9(0.1)	61.8(2.9)
Baoding	spring	294	207	87	7.9(0.3)	4	6	10	38(2.3)	-0.6(0.2)	122.2(6.9)
	summer	378	250	128	9.6(0.3)	5	8	12	35.1(2.1)	-0.7(0.2)	91.4(4.9)
	autumn	289	231	58	13(0.5)	7	12	18	54.7(3.7)	-0.6(0.2)	109.1(4.7)
	winter	321	255	66	11.1(0.4)	5	9	17	70.7(3.7)	-0.9(0.2)	107.6(7.2)

Table 1: Summary statistics of selected calm episodes in four different clusters from March 2013 to February 2019, including the total number and the numbers of episodes which began during the Day (6 am-6 pm) and at the Night (7 pm-5 am), the average, 25%, 50% and 75% quantiles of the Length of the episodes, the average Range (the difference between the maximum and minimum PM$_{2.5}$ in the calm episode, μg/m^3), the average $t_s - t_\omega$ (hours) between the episode's start and the ending time t_ω of a northerly cleaning process and the average Gap Time (hours) between two consecutive episodes with the standard error in the parentheses.

more frequent in winter. The numbers of calm episodes in Baoding were less than those of the other two cities, which was largely due to generally weaker northerly wind in Baoding as shown in panel (d) of Figure S2. Table 1 also shows that the majority of calm episodes happened during the day (6 am-6 pm). For all the four site clusters, the average length of calm episodes was smallest in spring, which was around seven hours, due to more air turbulence in the more windy spring season in that part of China.

Figure S4 shows the seasonal distribution of $t_s - t_\omega$ for selected calm episodes of each cluster, while Figure S5 presents the radar plots that depict the distributions of the wind direction and speed four hours before $\min\{t_s, t_\omega\}$ and four hours after $\max\{t_s, t_\omega\}$, respectively, in spring of cluster Beijing SE. The wind distribution before $\min\{t_s, t_\omega\}$ is dominated by NW and NE, and the four hours after $\max\{t_s, t_\omega\}$ is dominated by SW and SE. The period between t_s and t_ω saw a drop in NW in both percentage and velocity. Furthermore, Figure 2 displays changes in the average meteorological variables in the four hours before and after the start of the calm episodes for cluster Beijing NW in each season. Similar figures for the other three clusters are provided in Figure S6 - S8. In general, we can find a common downward trend in BLH, TEMP and CNWS and an upward trend in DEWP, HUMI and CSWS after the calm episodes start. These characteristics are related to the build-up of pollutants in the calm episodes, which is in line with the conclusions in the existing literature about the effects of meteorological conditions on pollutant concentrations (Zheng et al., 2015). From Figure S9 we can find that the patterns of pollutants during the episodes with the beginning in two time periods, day (6 am-6 pm) and night (7 pm-5 am), are different. Meanwhile, more episodes happened in the day. Therefore, we only consider comparing the results of episodes which started between 6 am and 6 pm.
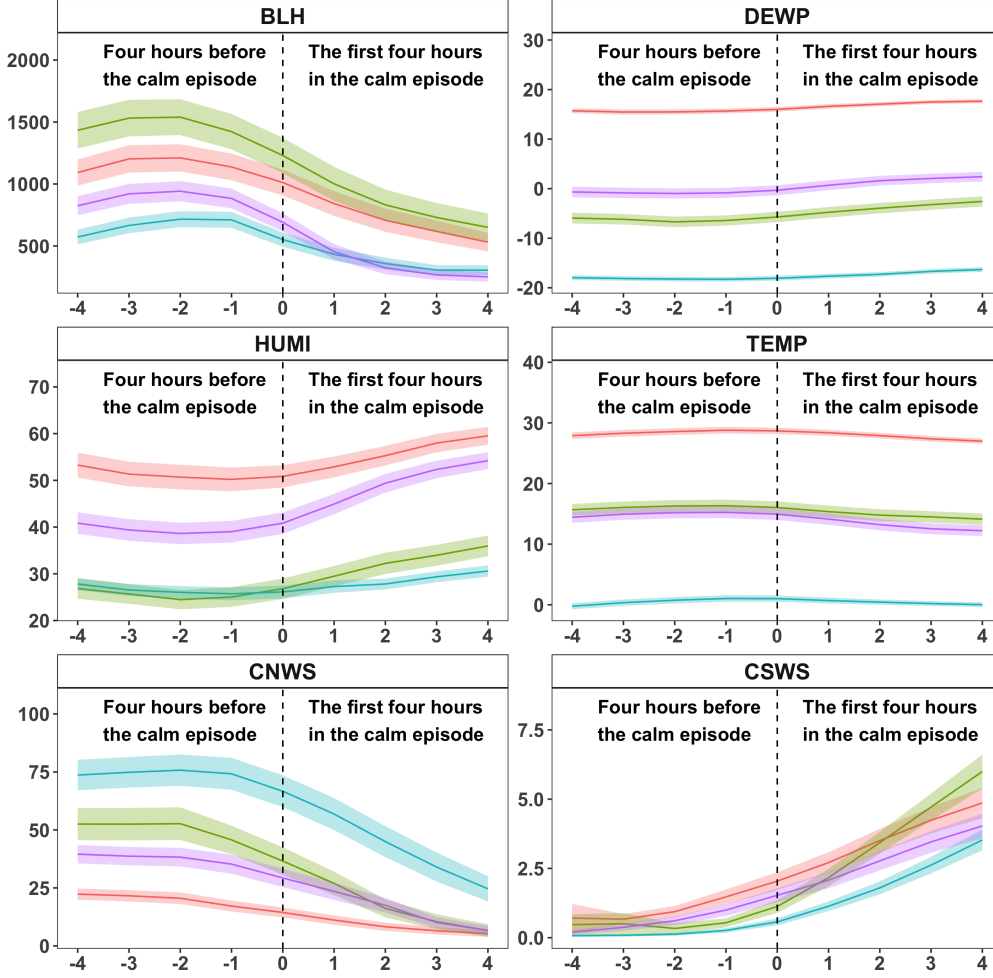
Figure 2: The average boundary layer height (BLH), dew point (DEWP), relative humidity (HUMI), temperature (TEMP), cumulative northerly wind speed (CNWS), and cumulative southerly wind speed (CSWS) in the four hours before and after the start of the calm episodes indicated by the dashed vertical line at zero in Beijing NW in spring (green), summer (red), autumn (purple) and winter (blue) with the 95% confidence intervals indicated by the colored areas.

4 Methods

4.1 Models for Calm Episodes

As shown in Table 1, the average length of the gap time between consecutive episodes was at least 60 hours in all seasons, and that in the non-winter seasons was even longer. Hence, different episodes may be regarded as independent, which leads us to consider a linear model for the growth of the pollutants during the episodes. It is noted that the sites within a cluster are quite close to each other, thus data from the three air-quality monitoring sites in a cluster are pooled to fit a common model for a season to make the analysis robust.

For a site cluster and a season, at an hour t in the j-th episode of year i, let Y_{ijt} be the concentration of a pollutant ($PM_{2.5}$, NO_2 or SO_2), $C_{ij} = (SNWS_{ij}, MCNWS_{ij})^\top$

Cluster	Variable	2013	2014	2015	2016	2017	2018	Average Rank	Average R^2	Average AIC	Average BIC
Beijing SE	Time dummies	1	1	1	1	1	2	1.2	0.68	1735	1800
	ΔLogBLH	—	2	—	2	2	5	5.2	0.70	1726	1795
	ΔDEWP	3	—	2	—	4	4	5.5	0.72	1700	1771
	MCNWS	—	4	—	—	3	1	6.3	0.75	1693	1768
	ΔPRES	2	3	—	—	6	—	6.8	0.77	1669	1747
	SNWS	4	—	—	—	—	3	7.8	0.78	1667	1748
	ΔTEMP	—	—	—	3	—	6	8.2	0.79	1661	1745
	ΔLogHUMI	—	—	4	—	5	—	8.2	0.81	1644	1732
	ΔCNWS	—	—	3	—	—	—	8.8	0.81	1645	1736
	ΔCSWS	—	—	5	—	—	—	9.2	0.81	1643	1737
Beijing NW	Time dummies	1	1	1	1	1	1	1.0	0.68	2145	2215
	ΔDEWP	2	—	4	—	3	2	5.2	0.71	2126	2199
	ΔPRES	—	4	2	—	—	4	6.7	0.72	2121	2197
	ΔTEMP	—	5	3	3	—	—	6.8	0.75	2092	2172
	MCNWS	—	2	—	—	2	—	7.3	0.76	2084	2167
	ΔCSWS	—	—	—	2	5	—	7.8	0.77	2078	2164
	ΔLogHUMI	—	6	—	—	—	3	8.2	0.78	2074	2165
	ΔCNWS	—	3	—	—	6	—	8.2	0.78	2068	2161
	SNWS	—	—	—	—	4	5	8.2	0.79	2067	2165
	ΔLogBLH	—	—	—	4	—	—	9.0	0.79	2065	2166
Tangshan	Time dummies	1	1	1	1	1	1	1.0	0.80	2401	2469
	ΔPRES	2	2	3	5	—	2	4.0	0.85	2327	2399
	SNWS	3	5	—	—	5	5	6.3	0.85	2321	2396
	ΔLogHUMI	—	4	—	2	4	—	6.7	0.86	2310	2389
	MCNWS	4	—	—	—	3	3	6.7	0.86	2300	2382
	ΔCSWS	—	—	—	4	2	6	7.0	0.87	2297	2383
	ΔDEWP	—	3	—	6	—	4	7.2	0.87	2283	2372
	ΔTEMP	—	—	2	—	—	—	8.7	0.88	2282	2375
	ΔLogBLH	—	—	—	3	—	—	8.8	0.88	2277	2374
	ΔCNWS	—	—	—	—	—	—	10.0	0.88	2277	2377
Baoding	Time dummies	1	1	1	1	1	1	1.0	0.81	2264	2341
	ΔPRES	—	2	3	—	2	2	4.8	0.83	2223	2303
	ΔLogHUMI	2	6	2	—	5	—	5.8	0.86	2157	2240
	ΔLogBLH	—	5	—	4	—	3	7.0	0.87	2153	2239
	ΔCNWS	—	—	—	3	3	6	7.0	0.87	2146	2236
	SNWS	—	3	—	—	6	5	7.3	0.87	2141	2235
	ΔCSWS	—	—	—	5	7	4	7.7	0.88	2132	2230
	ΔTEMP	3	—	4	—	—	—	7.8	0.88	2124	2225
	ΔDEWP	—	—	5	2	—	—	7.8	0.89	2109	2213
	MCNWS	—	4	—	—	4	—	8.0	0.89	2098	2206

Table 2: Variable ranks by the forward selection method for $PM_{2.5}$ in the spring of each year in different clusters during calm episodes and their average ranks, and the successive average R^2, AIC and BIC scores. A "-" indicates the selection was ended before the variable, which is given a rank of 10. The variables above the dashed line are those selected into the common baseline model according to the lowest average BIC.

be the two pre-episode variables, and

$$M_{ijt} = (\text{DEWP}_{ijt}, \text{PRES}_{ijt}, \text{TEMP}_{ijt}, \text{LogBLH}_{ijt}, \text{LogHUMI}_{ijt}, \text{CNWS}_{ijt}, \text{CSWS}_{ijt})^\top$$

be the vector of seven meteorological variables, for $i = 1, \cdots, A$, $j = 1, \cdots, n_i$ and $t = 0, \cdots, T_{ij}$. Here $A = 6$ is the total number of years in the study, n_i is the number of episodes in year i of the season in the site cluster, $t = 0$ corresponds to the starting time t_s of a calm episode defined in Section 3 and T_{ij} is the length of the j-th episode. Since the focus of the study is the pattern of pollution build-up in the episodes, we introduce a difference operator $\Delta A_{ijt} = A_{ijt} - A_{ij0}$ for a generic variable A. To reflect the hourly growth, we define $I_{ijt} = (I_{ijt}^1, I_{ijt}^3, \cdots, I_{ijt}^{T_{ij}})^\top$ of dummy variables for $1, 2, \cdots, T_{ij}$ hours after the episode starts for the time-effect. Then the model in year i for the lon-

gitudinal (panel) data in a cluster of a season is

$$\Delta Y_{ijt} = \Delta M_{ijt}^\top \beta_i + C_{ij}^\top \gamma_i + I_{ijt}^\top \eta_i + \epsilon_{ijt}, \tag{4.1}$$

where ϵ_{ijt} are possibly heterogeneous random errors with zero conditional mean and finite conditional variance given the explanatory variables. Let $\theta_i = (\beta_i^\top, \gamma_i^\top, \eta_i^\top)^\top$ be the $p \times 1$ vector of parameters, where p is the number of covariates. As the model parameters and their estimation are year, season and cluster specific, the year, season and cluster fixed effects are reflected in the parameters.

Model (4.1) allows heteroskedasticity and serial correlations in the error terms $\{\epsilon_{ijt}\}_{t=1}^{T_{ij}}$ that can be detected by the residual plot or tests (Breusch & Pagan, 1979; Wooldridge, 2010). In this study we use the OLS estimator for θ_i with the robust variance estimator for variance estimation to avoid potential misspecifications on the dynamic structure of $\{\epsilon_{ijt}\}_{t=1}^{T_{ij}}$ (Beck & Katz, 1995).

Let $\tilde{T}_i = \max_j T_{ij}$ be the maximum length of episodes in year i. As there are $\tilde{T}_i + 9$ candidate covariates in the panel regression, to avoid model over-fitting, we first select the important variables by the forward step-wise method based on the Bayesian information criterion (BIC) (Hastie et al., 2008), which chooses one variable at each step that leads to the largest reduction in the BIC until none variable can be added to reduce the BIC. Since the length of calm episodes varies, we regard the time dummies as a whole in the forward selection. Table 2 reports the selected variables and their order of selection for $PM_{2.5}$ in spring. It is shown that the time dummies were the most important one and were always selected first, and there was much accordance in the variable importance for the growth of a pollutant among different site clusters at a season. Table 3 summarizes the relative frequencies of the selected variables for the three pollutants in the four seasons in 2013-2018. It shows that PRES, DEWP and TEMP were key variables for the growth of $PM_{2.5}$ in the calm episodes. Besides, the pre-episode variable SNWS was also significant for the growth of $PM_{2.5}$ in autumn and winter. TEMP, BLH and HUMI were important for the growth of NO_2. As for the growth of SO_2, HUMI and BLH were important with TEMP, SNWS and MCNWS also selected frequently in autumn and winter. Figure S10-12 present estimates for the year, season and cluster specific coefficients of selected variables in the model for each pollutant. All predictors have been standardized before the estimation so that the estimates are directly comparable, which confirms the importance of variables shown in Table 3 and implies a generally strong and positive effect of DEWP and HUMI on pollutant concentrations as well as the negative effect of the pre-episode variables.

The subsequent analyses are based on the selected variables under Model (4.1). Without causing confusion, the selected meteorological and pre-episode variables are denoted as ΔM_{ijt} and C_{ij}, respectively. Let $X_{ijt} = (\Delta M_{ijt}^\top, C_{ij}^\top, I_{ijt}^\top)^\top$ be the vector of selected covariates at time t for episode j in year i. The OLS estimator for θ_i is

$$\hat{\theta}_i = \left(\sum_{j=1}^{n_i} \sum_{t=1}^{T_{ij}} X_{ijt} X_{ijt}^\top\right)^{-1} \sum_{j=1}^{n_i} \sum_{t=1}^{T_{ij}} X_{ijt} \Delta Y_{ijt}.$$

It is shown in the SI that under some assumptions, $\hat{\theta}_i$ is unbiased and consistent for θ_i with the asymptotic normality. To estimate the variance of OLS estimator $\hat{\theta}_i$ in the case of heteroskedastic and serial correlated errors $\{\epsilon_{ijt}\}$, several robust variance estimators for panel data regression have been proposed (Arellano, 1987; K.-Y. Liang & Zeger, 1986; White, 1980). In consideration of the unbalanced panels (different lengths of the episodes) in our setting, we use the robust variance estimator

$$\widehat{\mathrm{Var}}(\hat{\theta}_i) = \left(\sum_{j=1}^{n_i} \sum_{t=1}^{T_{ij}} X_{ijt} X_{ijt}^\top\right)^{-1} \left[\sum_{j=1}^{n_i} \left(\sum_{t=1}^{T_{ij}} X_{ijt} \hat{\epsilon}_{ijt}\right) \left(\sum_{t=1}^{T_{ij}} X_{ijt} \hat{\epsilon}_{ijt}\right)^\top\right] \left(\sum_{j=1}^{n_i} \sum_{t=1}^{T_{ij}} X_{ijt} X_{ijt}^\top\right)^{-1}, \tag{4.2}$$

where $\hat{\epsilon}_{ijt} = \Delta Y_{ijt} - X_{ijt}^\top \hat{\theta}_i$ is the OLS residual.

(a) PM$_{2.5}$

Spring	Time dummies 1	ΔPRES 1	ΔDEWP 0.75	ΔTEMP 0.5	ΔLogHUMI 0.5	ΔLogBLH 0.5	SNWS 0.5	ΔCSWS 0.5	MCNWS 0.5	ΔCNWS 0.25
Summer	Time dummies 1	ΔPRES 1	ΔTEMP 0.75	ΔLogBLH 0.75	ΔDEWP 0.75	ΔLogHUMI 0.5	ΔCSWS 0.5	SNWS 0.25	MCNWS 0.25	ΔCNWS 0.25
Autumn	Time dummies 1	SNWS 1	ΔTEMP 0.75	ΔDEWP 0.75	ΔLogHUMI 0.5	ΔPRES 0.5	ΔLogBLH 0.5	ΔCSWS 0.5	MCNWS 0.25	ΔCNWS 0.25
Winter	Time dummies 1	ΔTEMP 1	SNWS 1	ΔLogHUMI 0.75	ΔPRES 0.5	ΔLogBLH 0.5	ΔDEWP 0.5	MCNWS 0.5	ΔCSWS 0.25	ΔCNWS 0

(b) NO$_2$

Spring	Time dummies 1	ΔTEMP 1	ΔLogBLH 1	ΔLogHUMI 0.75	ΔPRES 0.5	SNWS 0.5	ΔCSWS 0.5	ΔDEWP 0.25	ΔCNWS 0.25	MCNWS 0
Summer	Time dummies 1	ΔTEMP 1	ΔPRES 1	ΔLogHUMI 0.75	ΔCSWS 0.75	MCNWS 0.5	ΔCNWS 0.5	ΔLogBLH 0.25	SNWS 0.25	ΔDEWP 0
Autumn	Time dummies 1	ΔLogHUMI 1	ΔLogBLH 1	ΔPRES 0.75	ΔCNWS 0.75	ΔTEMP 0.5	ΔCSWS 0.5	MCNWS 0.5	SNWS 0	ΔDEWP 0
Winter	Time dummies 1	ΔTEMP 1	ΔLogHUMI 1	ΔLogBLH 0.75	SNWS 0.75	ΔCSWS 0.5	ΔDEWP 0.5	ΔPRES 0.25	ΔCNWS 0.25	MCNWS 0

(c) SO$_2$

Spring	Time dummies 1	ΔPRES 1	ΔLogBLH 0.75	ΔCSWS 0.75	ΔTEMP 0.5	ΔLogHUMI 0.5	SNWS 0.5	ΔDEWP 0.5	MCNWS 0.5	ΔCNWS 0
Summer	ΔPRES 1	Time dummies 0.75	ΔLogBLH 0.75	SNWS 0.75	ΔCSWS 0.75	ΔLogHUMI 0.5	ΔDEWP 0.5	MCNWS 0.5	ΔTEMP 0.25	ΔCNWS 0.25
Autumn	Time dummies 1	ΔLogHUMI 1	SNWS 1	ΔTEMP 0.75	ΔLogBLH 0.75	ΔPRES 0.5	MCNWS 0.5	ΔDEWP 0.25	ΔCNWS 0.25	ΔCSWS 0
Winter	Time dummies 1	ΔLogHUMI 1	MCNWS 1	ΔTEMP 0.75	ΔLogBLH 0.75	ΔDEWP 0.5	ΔCNWS 0.5	ΔPRES 0.25	SNWS 0.25	ΔCSWS 0

Table 3: Relative frequencies of variables being selected within the first six steps of the forward selection procedure for the four seasons and three pollutants.

4.2 Meteorological Adjustment

As meteorological variables are subject to yearly variations, we need to adjust for such variation in order to compare fairly the pollution growth characteristics within episodes among different years. Doing so would make the estimated growth rates within episodes reflect the local emission rather than the meteorological profiles. We extend the adjustment framework established in X. Liang et al. (2015) and Zhang et al. (2020) for the current episode-based analysis by constructing meteorological baseline distributions for each season and cluster.

As the calm episodes have different lengths, let n_{il} denote the number of episodes whose length is l hours for a site cluster and a season in year i. Let $U_{ijt} := (\Delta M_{ijt}^{\top}, C_{ij}^{\top})^{\top}$ be the meteorological variables used in Model (4.1). We assume the episodes with the same length share the same meteorological distribution and define a set of positive probability weights $\{p_{il}\}_{l=3}^{\tilde{T}_i}$ that adds up to one and is subject to $\frac{n_{il}}{n_i} \to p_{il}$ as $n_i \to \infty$ for any $3 \le l \le \tilde{T}_i$ in a site cluster and a season of year i.

Let $f_{it}(u|l)$ be the conditional density of U_{ijt} given $T_{ij} = l$ for $t \le l$. Then, the density $f_{it}(u)$ of U_{ijt} at hour t in a site cluster and a certain season of year i is a mix-

ture of the densities with different lengths of episodes not smaller than t, namely

$$f_{it}(u) = (\sum_{l \geq t} p_{il})^{-1} \sum_{l \geq t} p_{il} f_{it}(u|l).$$

Let $\mu_{it}(\Delta m_{ijt}, c_{ij}) := \mathbb{E}(\Delta Y_{ijt}|\Delta M_{ijt} = \Delta m_{ijt}, C_{ij} = c_{ij}) = \Delta m_{ijt}^\top \beta_i + c_{ij}^\top \gamma_i + I_t^\top \eta_i$, where I_t is a $\tilde{T}_i$ dimensional vector of which all elements are 0 except the t-th element equals 1. Then, the average concentration at hour t of the episode is

$$\mathbb{E}(\Delta Y_{ijt}) = \int \mu_{it}(u) f_{it}(u) du.$$

However, the above average based on the density $f_{it}(u)$ of year i is confounded by the meteorological condition of year i. A version that is free of the confounding is needed.

In consideration of the unbalanced data panels, we focus on the adjustment at hours $t = 1, \cdots, \min_{1 \leq a \leq A} \tilde{T}_a$ so that the data of all A years can be utilised for the baseline meteorological construction. A solution to remove the yearly meteorological confounding is to replace $f_{it}(u)$ by an equally weighted density over A years:

$$f_{\cdot t}(u) = \frac{1}{A} \sum_{a=1}^A f_{at}(u) = \frac{1}{A} \sum_{a=1}^A (\sum_{l \geq t} p_{al})^{-1} \sum_{l \geq t} p_{al} f_{at}(u|l), \tag{4.3}$$

which defines the baseline meteorological condition over the A (identical to 6 here) years.

The adjusted average at time t in year i is the mean of ΔY_{ijt} for $U_{ijt} \sim f_{\cdot t}(u)$, that is

$$\mu_{it}^* = \int \mu_{it}(u) f_{\cdot t}(u) du = \frac{1}{A} \sum_{a=1}^A (\sum_{l \geq t} p_{al})^{-1} \sum_{l \geq t} p_{al} \int \mu_{it}(u) f_{at}(u|l) du$$

$$= I_t^\top \eta_i + \frac{1}{A} \sum_{a=1}^A (\sum_{l \geq t} p_{al})^{-1} \sum_{l \geq t} p_{al} \mathbb{E}(\Delta M_{ajt}|T_{aj} = l)^\top \beta_i \tag{4.4}$$

$$+ \frac{1}{A} \sum_{a=1}^A (\sum_{l \geq t} p_{al})^{-1} \sum_{l \geq t} p_{al} \mathbb{E}(C_{aj}|T_{aj} = l)^\top \gamma_i.$$

The meteorologically adjusted mean μ_{it}^* can be estimated by

$$\hat{\mu}_{it}^* = I_t^\top \hat{\eta}_i + \left(\frac{1}{A} \sum_{a=1}^A \frac{1}{\sum_{l \geq t} n_{al}} \sum_{s:T_{as} \geq t} \Delta M_{ast}^\top \right) \hat{\beta}_i + \left(\frac{1}{A} \sum_{a=1}^A \frac{1}{\sum_{l \geq t} n_{al}} \sum_{s:T_{as} \geq t} C_{as}^\top \right) \hat{\gamma}_i, \tag{4.5}$$

which makes the concentration during the calm episodes in different years comparable and reflects changes in the underlying emission.

In the SI, we provide the consistency, the asymptotic normality and the variance estimation of $\hat{\mu}_{it}^*$ for any $i = 1, \cdots, A$ and $\hat{\mu}_{it}^* - \hat{\mu}_{i't}^*$ for any $i \neq i'$ as $\min_{1 \leq a \leq A} n_a \to \infty$ under some assumptions, which can be used to test if any two years' growth rates were the same or not. We choose the growth rate in the first T hours of the episodes μ_{iT}^*/T as the criterion to compare the pollution growth in different years.

5 Results and Analyses

Using Model (4.1) with the selected variables and the meteorological adjustment approach, we obtain the within-episode growth patterns for $PM_{2.5}$, NO_2 and SO_2 in the four site clusters. Figure 3 displays the meteorologically adjusted growth curves $\hat{\mu}_{it}^*$ with

the 95% confidence intervals for the first six hours of episodes in the four seasons of years 2013-2018 for Beijing NW. Figures for other site clusters and pollutants are provided in Figure S13-S23 of the SI. It is noted that the smallest 25%, 50% and 75% quantiles of the episode lengths among the four site clusters for each season (Table 1) were 4, 6 and 9 hours, respectively. We chose the first six hours to ensure at least half of the data being used to construct the growth curves and to build the baseline meteorological distributions. The raw growth curves by directly averaging the hourly concentrations of the episodes are also shown in Figure 3. While most of the adjusted curves were close to the raw ones, there were occasions, for instance, spring of 2014 and 2018 and summer and
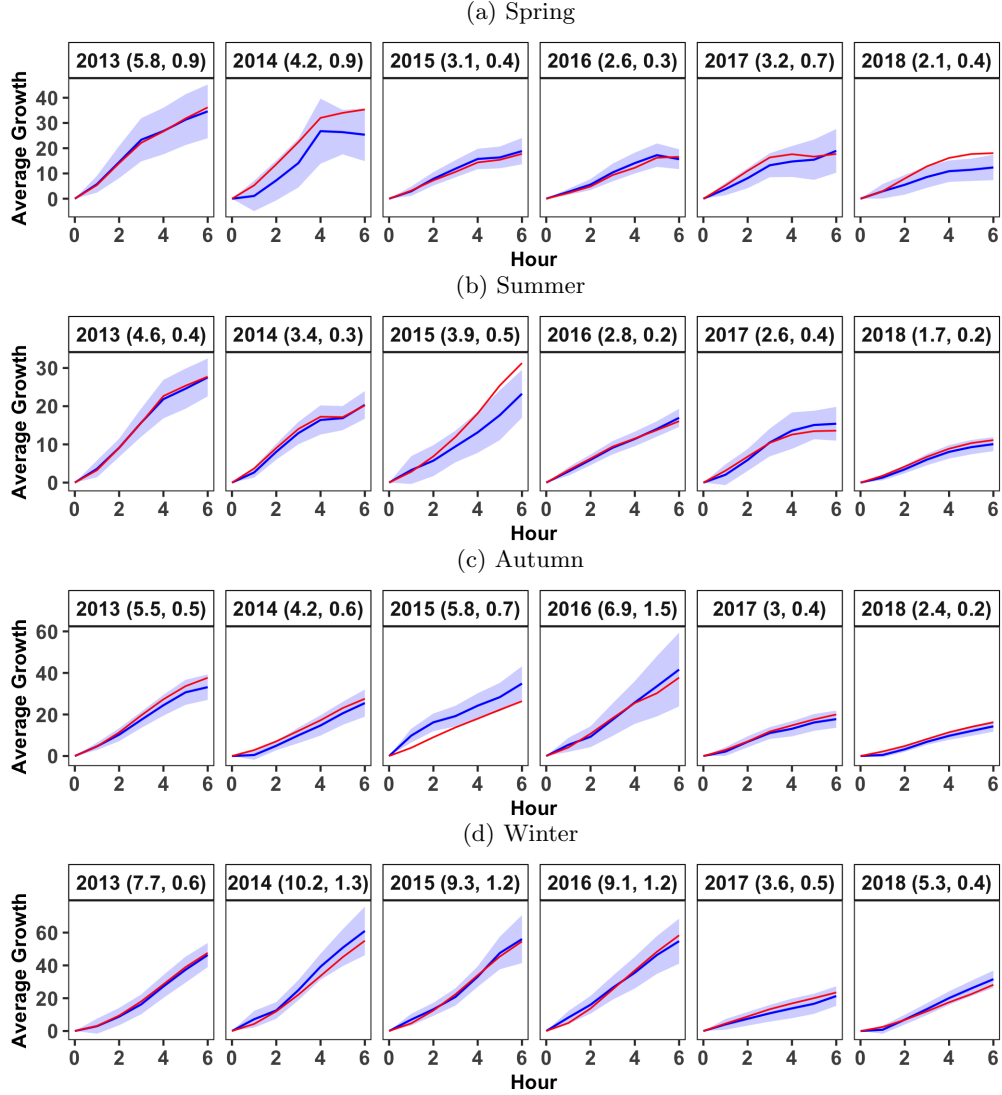
Figure 3: The adjusted (blue) and original (red) average growth ($\mu g/m^3$) of $PM_{2.5}$ in the first six hours of the calm episode for cluster Beijing NW in (a) spring (b) summer (c) autumn and (d) winter of six years. The 95% confidence intervals of adjusted averaged change of $PM_{2.5}$ are indicated by shading. And the adjusted average growth rate ($\mu g/m^3$ per hour) in the first six hours of the episodes that is the slope of the line between the first point and the last point on the curve of adjusted average growth as well as standard errors is marked in the parentheses.

fall of 2015, where the discrepancies between two curves for $PM_{2.5}$ were substantial. Figures S16 to S19 in the SI also displayed larger discrepancies for NO_2. The meteorological adjustment avoids the likely meteorological confounding. Figure 3 and the similar figures in the SI display monotone growth in the episodes with increased volatility. In most situations, the growth pattern was largely linear in the early hours with some tapering off toward the six hour cut-off. Table S2 in the SI reports the detailed 6-hour growth rates for all three pollutants and four site clusters.
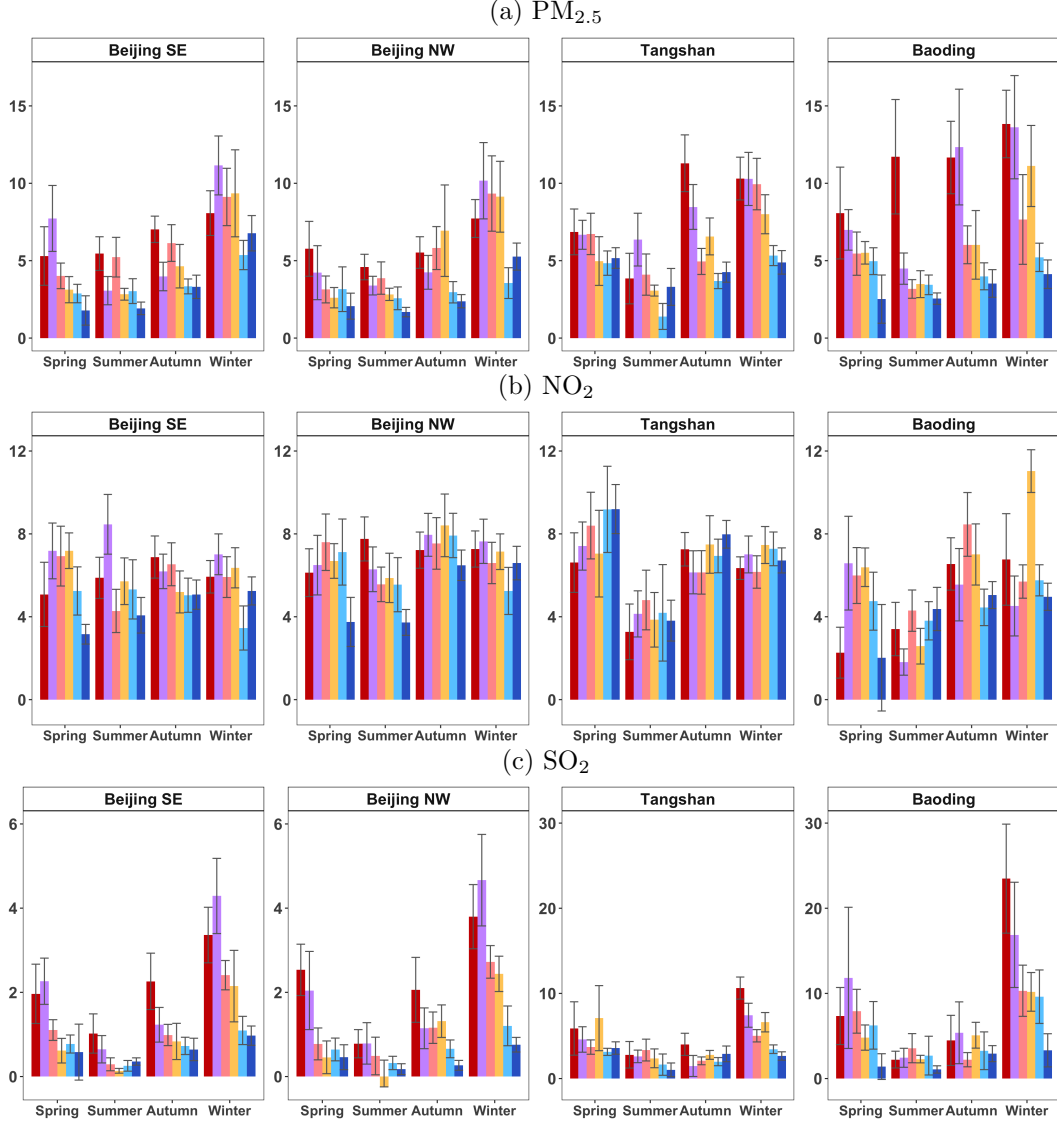
(a) $PM_{2.5}$

(b) NO_2

(c) SO_2

Figure 4: The adjusted average growth rate ($\mu g/m^3$ per hour) of (a) $PM_{2.5}$, (b) NO_2 and (c) SO_2 in the first six hours of the episodes for four clusters in four seasons of six seasonal years, 2013 (red), 2014 (purple), 2015 (pink), 2016 (yellow), 2017 (light blue), 2018 (blue) with the bars indicating the 95% confidence intervals.

Figure 4 displays the average growth rates $\hat{\mu}_{i6}^*/6$ within the first six hours of the calm episodes for the three pollutants and the four site clusters. It shows different seasonal patterns in the local emission, with the growth rates in winter being the largest and those in the summer the smallest for $PM_{2.5}$ and SO_2, while the seasonal variation

for NO_2 in Beijing was the least among the three cities. It also indicates temporal declines in the growth rates for $PM_{2.5}$ and SO_2 in all four seasons, with the most significant declines happened in winter in all four site clusters. The largest declines happened in winter 2017 for $PM_{2.5}$ and winter 2018 for SO_2 in Beijing, and in winter 2018 in Baoding for both $PM_{2.5}$ and SO_2. The declines in $PM_{2.5}$ and SO_2 were largely driven by a significant reduction in coal consumption and improvements in the coal combustion processes in North China. It is surprising to see that the winter growth rates of $PM_{2.5}$ in Beijing were comparable to those in the heavy industrial Tangshan and Baoding. Alarmingly, the 2018's winter $PM_{2.5}$ growth rates in Beijing's two site clusters were all higher than their Hebei peers.

In contrast to the general reduction in local emission related to $PM_{2.5}$ and SO_2, there had been no significant reduction in NO_2 related emission in all three cities. Indeed, for all city clusters and seasons, no significant reduction in the growth rate of NO_2 occurred earlier than that of $PM_{2.5}$. A substantial portion of the Tangshan's NO_2 came from its huge steel making activities (91.2 million tonnes in 2017, accounting for more than 11% of China's and 5% of the world production), and its much lower NO_2 growth rate in summer reflects the annual cycle in the steel production. However, for non-summer seasons, the growth rates in Tangshan were quite similar to those in the two site clusters in Beijing, except being slightly higher in the spring. As Beijing has no major industrial activities, these suggest that Beijing's 5-6 million cars' emissions from 2013-2018 generated as much NO_2 as the 2 millions vehicles plus the steel making activities in Tangshan. Beijing's NO_2 growth rates out-numbered those in Baoding in almost all seasons and years. These highlight the enormous contribution of Beijing's huge vehicle fleet for NO_x and then to $PM_{2.5}$ and O_3 generation.

Figure 5 displays the difference series between the adjusted 6-hour average growth rates of the three pollutants in 2014-2018 and those in 2013, which confirm the temporal patterns displayed in Figure 4 and provides more detailed information on the timing and the extent of the temporal changes in the 6-hour growth rates; Table S3 in the SI provides more details. For $PM_{2.5}$, the significant reduction in summer and fall mostly happened in 2014 in the four site clusters, with the exception in summer for Tangshan and fall for Baoding, which was delayed to 2017 and 2015, respectively. For spring, declines in the $PM_{2.5}$ growth rates took place for Beijing SE, Tangshan and Baoding in 2016, but earlier in 2015 for Beijing NW. For winter, the growth rates in two site clusters of Beijing started to reduce in 2017, while those in Tangshan and Baoding happened 1-2 years earlier. In summary, the declines in growth rates in $PM_{2.5}$ has been established for all seasons and all site clusters by 2017.

For all seasons except the winter in Beijing, the slowing down in the average growth rates of $PM_{2.5}$ over the levels in 2013 was extended in 2016-2017. However, in winter 2018, the slowing down was reversed by 1.4-1.7 $\mu g/m^3$ over the same period in 2017 in both site clusters in Beijing. The reduction in the growth rates of SO_2 as compared with those in 2013 was the most pronounced in winter with all four clusters started to see significant decline no later than 2015. Beijing was the earliest city that saw a significant reduction in spring and fall no later than 2015, while its summer decline came one year later in 2016 for Beijing NW. Baoding's SO_2 did not show a significant decrease from spring to fall before 2018. Tangshan faired better than Baoding for the SO_2 reduction, but the spring and summer reduction still came quite later. These show variation among the three cities in reducing the local emission related to the SO_2. However, the situation of NO_2 pollution was rather disappointing. A significant reduction in the spring and winter of Beijing did not happen before 2017. Tangshan's NO_2 growth actually increased over the 2013 level in recent years. The average reductions in both absolute and relative terms in the 6-hour average growth rates in years 2014-2018 over those in 2013 are reported in Table S3, which supports the result in Figure 4. The changes in adjusted av-
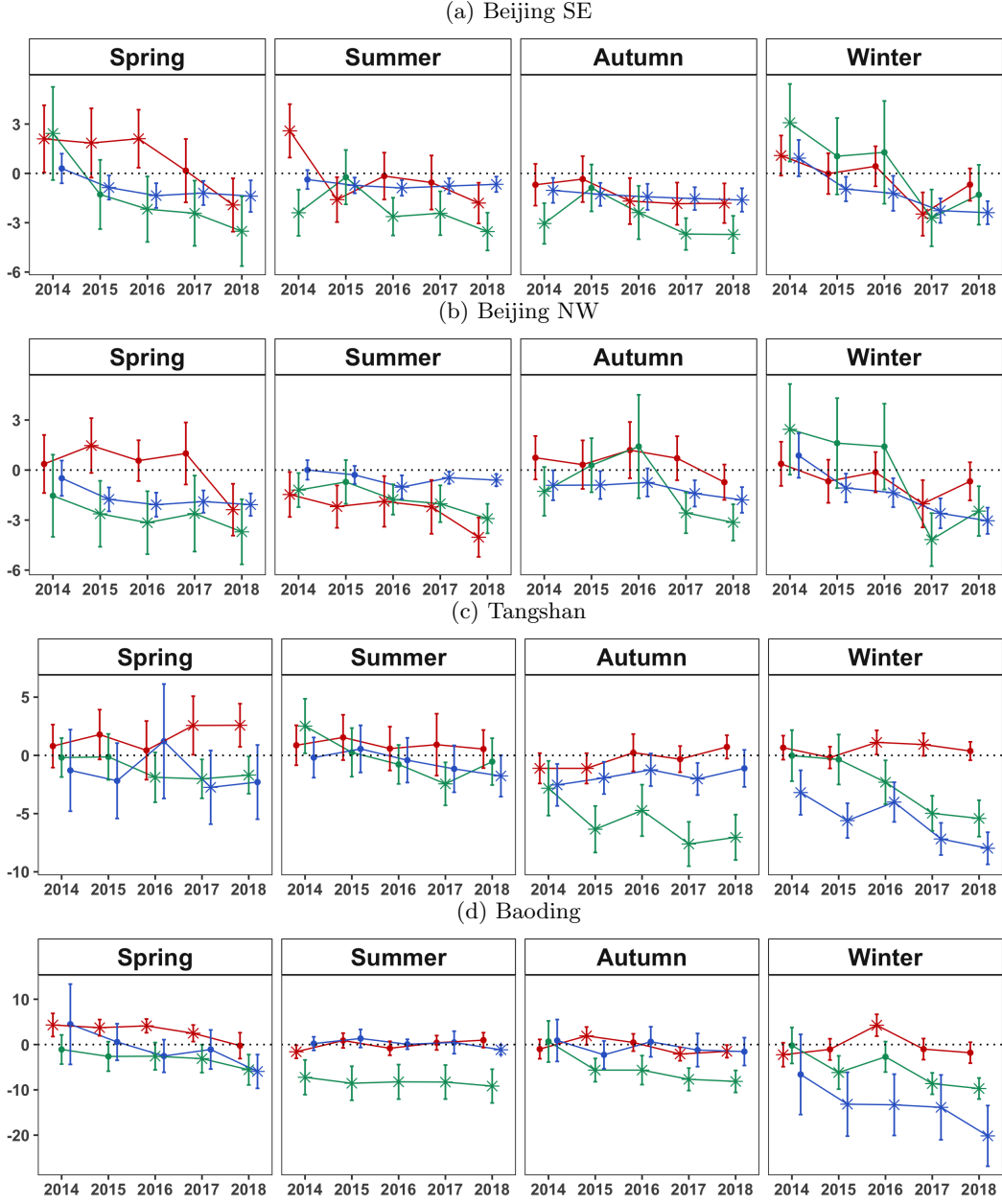
(a) Beijing SE

(b) Beijing NW

(c) Tangshan

(d) Baoding

Figure 5: Seasonal differences in the average adjusted growth rates ($\mu g/m^3$ per hour) of $PM_{2.5}$ (green), NO_2 (red) and SO_2 (blue) in the first six hours of the calm episodes between years 2014-2018 and 2013 with the 95% confidence intervals. The significant (non-significant) differences away from zero at the 5% level with one-sided alternative are marked by asterisks (points), respectively.

erage growth rates for each year relative to the levels in 2013 are listed in Table S2 whose results are summarized at the end of the introduction.

6 Discussion

In order to measure the local emission, we construct an algorithm to distract calm episodes from monitoring time series, which happened after sustained cleaning by the pollution-reducing wind to gauge local emission in a city and avoided regional transportation. The calm episode selection algorithm is much motivated by the geographical reality in North China. The algorithm can be applied to other locations in the world by replacing the northerly vs southerly regimes corresponding to the air pollutants' removal and transportation with ones suitable to the particular location. The statistical model and analysis for estimating the growth rates stay the same.

Our results on the meteorologically adjusted growth rates of the three pollutants are consistent with some published results, for instance, the revelation of an increased contribution of vehicle exhaust to $PM_{2.5}$ concentrations in the Beijing–Tianjin–Hebei region from 19% in March 2013 to 54% in March 2018 (Z. Chen et al., 2019) and the findings in T. Huang et al. (2017); C.-S. Liang et al. (2020). Figure S24-27 demonstrate that our main conclusions are also in accordance with the trend of the official statistics on energy consumption, outputs of heavy industry products and the aggregated emission estimates released by Municipal Bureau of Statistics and NBS Survey Office in three cities since 2013. The declined growth rates in SO_2 and $PM_{2.5}$ were mostly the result of sustained effort in cleaner combustion of coal and forbidding domestic use of coal for cooking and winter heating over the NCP (H. Chen & Chen, 2019). The lack of improvement in the NO_2 growth rate reflects a dilemma that the three cities have been facing in controlling emissions from their ever increasing motor vehicle fleets. Clearly, the policies having been put in place in recent years to control motor vehicle emissions, which include making every domestic car off the road one day per working week and upgrading the fuel emission standards, are insufficient to cut back the NO_2 growth rates. The stubborn NO_2 situation explained the sustained O_3 rise in the NCP (L. Chen et al., 2018), which should encourage city authorities to unveil policies to reduce the growth rate of NO_2 that can lead to a further decline in $PM_{2.5}$.

7 Author contributions

Zhu constructed the episode selection algorithm and performed the analyses while assisted by Liang. Chen envisaged the study and led the design and execution of the project. Chen and Zhu wrote the manuscript, and all three authors gave final approval for publication.

Data Availability Statement

The authors declare that data sets for this research are available in the following online repository. The ERA5 hourly data used in this study were collected from the ECMWF website (`https://cds.climate.copernicus.eu/cdsapp$\#$!/dataset/reanalysis -era5-single-levels?tab=overview`). The pollution data are in the repository (`https:// archive.ics.uci.edu/ml/datasets/Beijing+Multi-Site+Air-Quality+Data`). Data about the official statistics on energy consumption, outputs of heavy industry products and pollutant emissions are available through Baoding Municipal Bureau of Statistics, NBS Survey Office in Baoding (2019, 2020); Beijing Municipal Bureau of Statistics, NBS Survey Office in Beijing (2019, 2020); Tangshan Municipal Bureau of Statistics, NBS Survey Office in Tangshan (2020a, 2020b).

References

Arellano, M. (1987). Computing robust standard errors for within-groups estimators. *Oxford Bulletin of Economics and Statistics*, *49*(4), 431-434. Retrieved from `https://ideas.repec.org/a/bla/obuest/v49y1987i4p431-34.html`

Baoding Municipal Bureau of Statistics, NBS Survey Office in Baoding. (2019). *Baoding economy statistical yearbook 2019.* China Statistical Press, Beijing, China. Retrieved from `https://navi.cnki.net/KNavi/YearbookDetail?pcode=CYFD&pykm=YBDJJ&bh` (Last access: 12 October 2020)

Baoding Municipal Bureau of Statistics, NBS Survey Office in Baoding. (2020). *Statistical Communiqué on the National Economy and Social Development of Baoding in 2019.* `http://www.bd.gov.cn/zwgknr-888888008-235449.html`. (Last access: 12 October 2020)

Beck, N., & Katz, J. N. (1995). What to do (and not to do) with time-series cross-section data. *The American Political Science Review*, *89*(3), 634–647. Retrieved from `http://www.jstor.org/stable/2082979`

Beijing Municipal Bureau of Statistics, NBS Survey Office in Beijing. (2019). *Beijing statistical yearbook 2019.* China Statistical Press, Beijing, China. Retrieved from `http://nj.tjj.beijing.gov.cn/nj/main/2019-tjnj/zk/indexeh.htm` (Last access: 12 October 2020)

Beijing Municipal Bureau of Statistics, NBS Survey Office in Beijing. (2020). *Statistical Communiqué on the National Economy and Social Development of Beijing in 2019.* `http://tjj.beijing.gov.cn/EnglishSite/`. (Last access: 12 October 2020)

Breusch, T. S., & Pagan, A. R. (1979). A simple test for heteroscedasticity and random coefficient variation. *Econometrica*, *47*(5), 1287–1294. Retrieved from `http://www.jstor.org/stable/1911963`

Chen, H., & Chen, W. (2019). Potential impact of shifting coal to gas and electricity for building sectors in 28 major northern cities of China. *Applied Energy*, *236*, 1049 - 1061. Retrieved from `http://www.sciencedirect.com/science/article/pii/S0306261918318695` doi: https://doi.org/10.1016/j.apenergy.2018.12.051

Chen, L., Guo, B., Huang, J., He, J., Wang, H., Zhang, S., & Chen, S. X. (2018). Assessing air-quality in Beijing-Tianjin-Hebei region: The method and mixed tales of PM2.5 and O3. *Atmospheric Environment*, *193*, 290 - 301. Retrieved from `http://www.sciencedirect.com/science/article/pii/S1352231018305685`

Chen, Z., Chen, D., Wen, W., Zhuang, Y., Kwan, M.-P., Chen, B., ... Xu, B. (2019). Evaluating the "2 + 26" regional strategy for air quality improvement during two air pollution alerts in Beijing: variations in $PM_{2.5}$ concentrations, source apportionment, and the relative contribution of local emission and regional transport. *Atmospheric Chemistry and Physics*, *19*(10), 6879–6891. Retrieved from `https://acp.copernicus.org/articles/19/6879/2019/` doi: 10.5194/acp-19-6879-2019

Hastie, T., Tibshirani, R., & Friedman, J. (2008). The elements of statistical learning: Data mining, inference, and prediction. In (2nd ed., p. 58-60). Springer.

Huang, K., Zhuang, G., Wang, Q., Fu, J. S., Lin, Y., Liu, T., ... Deng, C. (2014). Extreme haze pollution in Beijing during January 2013: chemical characteristics, formation mechanism and role of fog processing. *Atmospheric Chemistry and Physics Discussions*, *14*(6), 7517–7556. Retrieved from `https://www.atmos-chem-phys-discuss.net/14/7517/2014/` doi: 10.5194/acpd-14-7517-2014

Huang, T., Zhu, X., Zhong, Q., Yun, X., Meng, W., Li, B., ... Tao, S. (2017). Spatial and temporal trends in global emissions of nitrogen oxides from 1960 to 2014. *Environmental Science & Technology*, *51*(14), 7992-8000. Retrieved from `https://doi.org/10.1021/acs.est.7b02235` doi: 10.1021/acs.est.7b02235

Huang, Y., Shen, H., Chen, Y., Zhong, Q., Chen, H., Wang, R., ... Tao, S. (2015). Global organic carbon emissions from primary sources from 1960 to 2009. *Atmospheric Environment*, *122*, 505 - 512. Retrieved from `http://www.sciencedirect.com/science/article/pii/S1352231015304362` doi: https://doi.org/10.1016/j.atmosenv.2015.10.017

Kuykendal, W. (2017). *Emissions Inventory Guidance for Implementation of Ozone and Particulate Matter National Ambient Air Quality Standards (NAAQS) and Regional Haze Regulations.* U.S. Environmental Protection Agency, Washington. Retrieved from `https://www.epa.gov/sites/production/files/2017-07/documents/ei_guidance_may_2017_final_rev.pdf`

Lee, S.-M., Princevac, M., Mitsutomi, S., & Cassmassi, J. (2009). MM5 simulations for air quality modeling: An application to a coastal area with complex terrain. *Atmospheric Environment*, *43*(2), 447 - 457. Retrieved from `http://www.sciencedirect.com/science/article/pii/S1352231008006614` doi: https://doi.org/10.1016/j.atmosenv.2008.07.067

Li, X., Zhang, Q., Zhang, Y., Zheng, B., Wang, K., Chen, Y., ... He, K. (2015). Source contributions of urban PM2.5 in the Beijing–Tianjin–Hebei region: Changes between 2006 and 2013 and relative impacts of emissions and meteorology. *Atmospheric Environment*, *123*, 229 - 239. Retrieved from `http://www.sciencedirect.com/science/article/pii/S1352231015304660` doi: https://doi.org/10.1016/j.atmosenv.2015.10.048

Liang, C.-S., Wu, H., Li, H.-Y., Zhang, Q., Li, Z., & He, K.-B. (2020). Efficient data preprocessing, episode classification, and source apportionment of particle number concentrations. *Science of The Total Environment*, *744*, 140923. Retrieved from `http://www.sciencedirect.com/science/article/pii/S0048969720344521` doi: https://doi.org/10.1016/j.scitotenv.2020.140923

Liang, K.-Y., & Zeger, S. L. (1986). Longitudinal data analysis using generalized linear models. *Biometrika*, *73*(1), 13–22. Retrieved from `http://www.jstor.org/stable/2336267`

Liang, X., Zou, T., Guo, B., Li, S., Zhang, H., Zhang, S., ... Chen, S. X. (2015). Assessing Beijing's PM2.5 pollution: severity, weather impact, APEC and winter heating. *Proceedings of the Royal Society A: Mathematical, Physical and Engineering Sciences*, *471*(2182), 20150257. Retrieved from `https://royalsocietypublishing.org/doi/abs/10.1098/rspa.2015.0257` doi: 10.1098/rspa.2015.0257

MEP. (2017). *2017 air pollution prevention and management plan for the Beijing-Tianjin-Hebei region and its surrounding areas.* `http://dqhj.mee.gov.cn/dtxx/201703/t20170323_408663.shtml`. (Last access: 12 October 2020)

Seo, J., Kim, J. Y., Youn, D., Lee, J. Y., Kim, H., Lim, Y. B., ... Jin, H. C. (2017). On the multiday haze in the Asian continental outflow: the important role of synoptic conditions combined with regional and local sources. *Atmospheric Chemistry and Physics*, *17*(15), 9311–9332. Retrieved from `https://acp.copernicus.org/articles/17/9311/2017/` doi: 10.5194/acp-17-9311-2017

Su, T., Li, J., Li, C., Lau, A. K.-H., Yang, D., & Shen, C. (2017). An intercomparison of AOD-converted PM2.5 concentrations using different approaches for estimating aerosol vertical distribution. *Atmospheric Environment*, *166*, 531 - 542. Retrieved from `http://www.sciencedirect.com/science/article/pii/S1352231017305034` doi: 10.1016/j.atmosenv.2017.07.054

Su, T., Li, Z., & Kahn, R. (2018, 11). Relationships between the planetary boundary layer height and surface pollutants derived from lidar observations over China: Regional pattern and influencing factors. *Atmospheric Chemistry and Physics*, *18*(21), 15921-15935. doi: 10.5194/acp-18-15921-2018

Tangshan Municipal Bureau of Statistics, NBS Survey Office in Tangshan. (2020a). *Statistical Communiqué on the National Economy and Social Development of*

Tangshan in 2019. `http://new.tangshan.gov.cn/zhengwu/tjxx/20200403/909974.html`. (Last access: 12 October 2020)

Tangshan Municipal Bureau of Statistics, NBS Survey Office in Tangshan. (2020b). *Tangshan statistical yearbook 2019.* China Statistical Press, Beijing, China. Retrieved from `http://new.tangshan.gov.cn/zhengwu/tjxx/20200519/909919.html` (Last access: 12 October 2020)

Tie, X., Madronich, S., Li, G., Ying, Z., Zhang, R., Garcia, A. R., ... Liu, Y. (2007). Characterizations of chemical oxidants in Mexico City: A regional chemical dynamical model (wrf-chem) study. *Atmospheric Environment*, *41*(9), 1989 - 2008. Retrieved from `http://www.sciencedirect.com/science/article/pii/S1352231006010399` doi: https://doi.org/10.1016/j.atmosenv.2006.10.053

Titov, M., Sturman, A. P., & Zawar-Reza, P. (2007). Application of MM5 and CAMx4 to local scale dispersion of particulate matter for the city of Christchurch, New Zealand. *Atmospheric Environment*, *41*(2), 327 - 338. Retrieved from `http://www.sciencedirect.com/science/article/pii/S1352231006008296` doi: https://doi.org/10.1016/j.atmosenv.2006.08.012

Wang, L., Zhang, N., Liu, Z., Sun, Y., Ji, D., & Wang, Y. (2014). The influence of climate factors, meteorological conditions, and boundary-layer structure on severe haze pollution in the Beijing-Tianjin-Hebei region during January 2013. *Advances in Meteorology*, *2014*(7), 1-14. doi: 10.1155/2014/685971

Wang, L. T., Wei, Z., Yang, J., Zhang, Y., Zhang, F. F., Su, J., ... Zhang, Q. (2014). The 2013 severe haze over southern Hebei, China: model evaluation, source apportionment, and policy implications. *Atmospheric Chemistry and Physics*, *14*(6), 3151–3173. Retrieved from `https://acp.copernicus.org/articles/14/3151/2014/` doi: 10.5194/acp-14-3151-2014

Wang, Z., Li, J., Wang, Z., Yang, W., Tang, X., Ge, B., ... Su, D. (2014). Modeling study of regional severe hazes over mid-eastern China in January 2013 and its implications on pollution prevention and control. *Science China Earth Sciences*, *57*(1), 3–13. doi: 10.1007/s11430-013-4793-0

White, H. (1980). A heteroskedasticity-consistent covariance matrix estimator and a direct test for heteroskedasticity. *Econometrica*, *48*(4), 817–838. Retrieved from `http://www.jstor.org/stable/1912934`

Wooldridge, J. M. (2010). Econometric analysis of cross section and panel data. In (2nd ed., p. 299-300). The MIT Press: The MIT Press.

Wu, D., Fung, J. C. H., Yao, T., & Lau, A. K. H. (2013). A study of control policy in the Pearl River Delta region by using the particulate matter source apportionment method. *Atmospheric Environment*, *76*, 147 - 161. Retrieved from `http://www.sciencedirect.com/science/article/pii/S1352231012011569` doi: https://doi.org/10.1016/j.atmosenv.2012.11.069

Xing, J., Wang, S. X., Jang, C., Zhu, Y., & Hao, J. M. (2011). Nonlinear response of ozone to precursor emission changes in China: a modeling study using response surface methodology. *Atmospheric Chemistry and Physics*, *11*(10), 5027–5044. Retrieved from `https://acp.copernicus.org/articles/11/5027/2011/` doi: 10.5194/acp-11-5027-2011

Yang, K., Dickerson, R. R., Carn, S. A., Ge, C., & Wang, J. (2013). First observations of SO2 from the satellite Suomi NPP OMPS: Widespread air pollution events over China. *Geophysical Research Letters*, *40*(18), 4957-4962. Retrieved from `https://agupubs.onlinelibrary.wiley.com/doi/abs/10.1002/grl.50952` doi: 10.1002/grl.50952

Zhang, S., Chen, S., Guo, B., Wang, H., & Lin, W. (2020). Regional air-quality assessment that adjusts for meteorological confounding. *SCIENTIA SINICA Mathematica*, *50*(4), 527. doi: 10.1360/SCM-2019-0368

Zhang, S., Guo, B., Dong, A., He, J., Xu, Z., & Chen, S. (2017). Cautionary tales on air-quality improvement in Beijing. *Proceedings of the Royal Society A: Mathe-*

matical, Physical and Engineering Science, *473*(2205), 20170457. doi: 10.1098/ rspa.2017.0457

Zheng, G. J., Duan, F. K., Su, H., Ma, Y. L., Cheng, Y., Zheng, B., ... He, K. B. (2015). Exploring the severe winter haze in Beijing: the impact of synoptic weather, regional transport and heterogeneous reactions. *At-mospheric Chemistry and Physics*, *15*(6), 2969–2983. Retrieved from `https://acp.copernicus.org/articles/15/2969/2015/` doi: 10.5194/ acp-15-2969-2015

Zhong, Q., Huang, Y., Shen, H., Chen, Y., Chen, H., Huang, T., ... Tao, S. (2017). Global estimates of carbon monoxide emissions from 1960 to 2013. *Environmental Science and Pollution Research*, *24*(1), 864–873. Retrieved from `https://doi.org/10.1007/s11356-016-7896-2` doi: https://doi.org/10.1007/s11356-016-7896-2